Hindawi
Journal of Electrical and Computer Engineering
Volume 2023, Article ID 9878434, 1 page
https://doi.org/10.1155/2023/9878434

*Retraction*

# Retracted: Fabrication and Sc-Refinement of $SiC_p$/A356 Composites by Vacuum Stirring Casting Method

**Journal of Electrical and Computer Engineering**

Received 15 August 2023; Accepted 15 August 2023; Published 16 August 2023



This article has been retracted by Hindawi following an investigation undertaken by the publisher [1]. This investigation has uncovered evidence of one or more of the following indicators of systematic manipulation of the publication process:

(1) Discrepancies in scope

(2) Discrepancies in the description of the research reported

(3) Discrepancies between the availability of data and the research described

(4) Inappropriate citations

(5) Incoherent, meaningless and/or irrelevant content included in the article

(6) Peer-review manipulation

The presence of these indicators undermines our confidence in the integrity of the article's content and we cannot, therefore, vouch for its reliability. Please note that this notice is intended solely to alert readers that the content of this article is unreliable. We have not investigated whether authors were aware of or involved in the systematic manipulation of the publication process.

Wiley and Hindawi regrets that the usual quality checks did not identify these issues before publication and have since put additional measures in place to safeguard research integrity.

We wish to credit our own Research Integrity and Research Publishing teams and anonymous and named external researchers and research integrity experts for contributing to this investigation.

The corresponding author, as the representative of all authors, has been given the opportunity to register their agreement or disagreement to this retraction. We have kept a record of any response received.

## References

[1] F. Chen and K. Wang, "Fabrication and Sc-Refinement of $SiC_p$/A356 Composites by Vacuum Stirring Casting Method," *Journal of Electrical and Computer Engineering*, vol. 2022, Article ID 5460706, 11 pages, 2022.

Hindawi
Journal of Electrical and Computer Engineering
Volume 2022, Article ID 5460706, 11 pages
https://doi.org/10.1155/2022/5460706



*Research Article*

# Fabrication and Sc-Refinement of $SiC_p$/A356 Composites by Vacuum Stirring Casting Method

**Fukun Chen and Kuangfei Wang**

*School of Materials Science and Engineering, Henan Polytechnic University, Jiaozuo 454003, China*

Correspondence should be addressed to Fukun Chen; cfk1998@home.hpu.edu.cn

Received 26 February 2022; Revised 21 March 2022; Accepted 9 April 2022; Published 21 April 2022

Academic Editor: Wei Liu



Aluminum matrix composites reinforced with 10 vol.% SiC particles ($SiC_p$/Al MMCs) were prepared throughthe vacuum stirring method from SiC particles preoxidated at high temperature, followed by posttreatments of remelting and Sc addition treatment. Major problems during vacuum stirring preparation were investigated. Results show that overoxidation of SiC particles may occur during the vacuum stirring process, which causes loss of SiC particles and increases in "impurity pores" after solidification or aggregation of SiC particles, leading to scarcely improved mechanical properties of the prepared $SiC_p$/Al composites. After Sc addition treatment, the $\alpha$-Al and eutectic Si phases were obviously refined. The composite matrix was strengthened. The result indicates that the maximum tensile strength of 10 vol.% $SiC_p$/A356 composites with Sc addition treatment was 193.5 MPa, which was increased by 43% compared with the matrix alloy. Moreover, a fracture at particles was detected after Sc addition treatment. The stress could be effectively transferred to the SiC particles when the fracture occurred.

## 1. Introduction

At present, $SiC_p$/Al composites have drawn great research interest in the material realm for their excellent physical properties, including high specific strength, high specific rigidity, high abrasive resistance, low thermal expansivity, and low manufacturing cost [1–3]. Several fabrication methodologies have been used for the production of aluminum matrix composites. Powder metallurgy (PM) processes are suitable for any alloy, and the composites are well combined and uniformly distributed. However, due to the high cost and complex preparation process, PM is not an ideal methodology for mass production [4, 5]. Spray deposition process has the characteristics of rapid solidification and the volume fraction of reinforcement is not limited, but the cost is high, and the porosity of the composites is large, which requires further processing and densification [6, 7].

Among processing methods for $SiC_p$/Al composites, the most concerned one is the melt stirring method for simplified preparation techniques and low cost [8, 9]. Currently, research on melt stirring processing mainly focuses on SiC particle modification and stirring processes. For example, Wu et al. [10] proposed an approach to improving the surface activity of SiC particles so as to increase the wettability of Al melt for SiC particles by coating a Ni-P layer on SiC particles through chemical plating. Hashim et al. [11] reported greatly enhanced wettability between SiC particles and A356 Al melt by the addition of Mg. As for the research on stirring processes, Prabu et al. [12] reported vacuum stirring produced metal matrix composites featuring uniform dispersion of particles within through optimization of processing parameters. There are many SiC preconditioning methods, among which the most adopted one is preoxidation on account of the simple procedure and low cost. However, during melt stirring processing, aggregation of SiC particles, inclusion in Al melt, and high gas content are common issues responsible for high porosity in aluminum matrix composites, which hinder the popularization of this method [13]. Herein, the causes for these problems in the preparation of A356 aluminum alloy composites through vacuum stirring are analyzed and discussed. Furthermore, the effect of rare earth element Sc on the remelted SiC

particle strengthened Al matrix composites was investigated. Hopefully, this work can provide a solid reference for the preparation of aluminum matrix composites and the application of rare earth element Sc in composites.

## 2. Materials and Methods

Aluminum matrix composites reinforced with 10 vol.% $SiC_p$ was produced by a vacuum stirring process. A356 cast aluminum alloy was selected as the matrix. The Sc content in Al-Sc intermediate alloy was 25 wt%. Table 1 shows the chemical compositions of A356 alloy, of which the 0.3 wt% of Mg is beneficial for the wetting of SiC particles in the aluminum melt.

SiC particles with an average size of about 10–20 $\mu$m are used as reinforcement, whose microstructure is shown in Figure 1(a). The surface of untreated SiC particles is smooth and with sharp edges. When the reinforcement particles have sharp edges, the bonding interface between the particles and the matrix is not strong during the process of adding the melt to prepare it into a composite material. When stress is applied, it is very easy to produce stress concentration in these areas, which becomes a source of cracks and causes damage to the physical properties of the material. Before adding to Al melt. SiC particles first underwent preconditioning to form a layer of $SiO_2$ on the surface of particles, where the powder was placed in a ceramic plate and heated in a heat treatment furnace at 1000°C for 6 h. The microstructure of oxidation-treated SiC particles is shown in Figure 1(b). After the high-temperature oxidation at 1000°C, the oxidation reaction of SiC particles is obvious, and the surface projections of the particles become thick, and the sharp edges of their edges appear obvious passivation and become rounded. Figure 1(c) shows the XRD pattern of SiC particles, and it proves that $SiO_2$ is generated after oxidation treatment at 1000°C for 6 h.

ZGS-50 vacuum multifunctional induction aluminum melting furnace was used for fabrication. Figure 2 shows the schematic of the vacuum furnace, whose vacuum degree is $1 \times 10^{-5}$ Pa, and the stirring device was made of heat-resisting Nb-Zr alloy.

Firstly, A356 aluminum ingots were heated to 760°C into melt under the intermediate frequency of 2000–2500 Hz in the graphite crucible inside the intermediate frequency furnace. Once the alloy melted, deslagging and degas were conducted and the upper tank was sealed and vaccumized to $1 \times 10^{-5}$ Pa. Subsequently, the experiments were carried out as follows: (1) vacuum stirring temperature was set at 750°C, 700°C, and 650°C, respectively, at a stirring speed of 300 r/min. The preconditioned 10 vol.% SiC particles were added to the Al melt in batches. Pure Ar gas was chosen as the carrier in the process of adding SiC particles to reduce the introduction of oxygen. Then vacuum degree of the furnace was evacuated to $1 \times 10^{-5}$ Pa again. The melt mixture was cast after 40 min of stirring. (2) The optimal composite determined in (1) was remelted in the vacuum furnace. Al-Sc intermediate alloy was added in proportion to the composites melt at the temperature of 700°C and 720°C, followed by 20 min of stirring at 150 r/min. The melt mixture was cast into a graphite mold after Ar washing and degassing. The whole process is protected by Ar gas to ensure that the atmosphere inside the furnace is always oxygen-free or low oxygen.

Table 1: Chemical composition of the A356 alloy.

| A356 | Si | Mg | Fe | Ti | Sr | B | Al |
|---|---|---|---|---|---|---|---|
| %composition | 6.83 | 0.34 | 0.07 | 0.11 | 0.024 | <0.001 | Balance |

After casting, the samples were taken out of the molds when cooled to room temperature and then wire-cut into tensile specimens (∅5 × 50 mm), metallographic specimens (10 × 10 × 10 mm), and hardness specimens. The metallographic specimens were successively sanded with #400, #800, #1000, and #1200 abrasive papers and polished on the metallographic polishing machine. After 10 min of ultrasonic cleaning in 1 : 1 ethanol/acetone solution, the polished specimens were corroded for 20 s by 10% HF ethanol solution. Finally, the specimens were washed with absolute ethanol, and the watermarks were dried with a blow-dryer. Metallographic imaging was observed by optical microscope (OLYMPUS-CK40M). Tensile properties were tested on a universal electronic testing machine (IIC-MST-100), and the strain rate was set to be 0.2 mm/min. The tensile property data were based on the average of four tests. Mh-5 microhardness tester was used to test the microhardness of the composites. The loading pressure was set at 500 g and the loading time was set at 5 s. The average value of 5 points measured was taken as the microhardness of the sample. Observation of the microstructure and fracture morphology of composites was carried out by scanning electron microscope (FEI Quanta 200), and $SiC_p$/Al interface reaction products were analyzed by energy-dispersive X-ray spectroscopy (EDS). The phase constituents of the composites were identified by X-ray diffraction (XRD, SmartLab, Rigaku Corporation, Tokyo, Japan) using Cu-Ka radiation with the following test conditions: tube voltage of 40 kV, tube current of 150 mA, scanning angle of 0–90°, step size of 0.02°, and scanning speed of 10°/min.

## 3. Results

*3.1. The Effects of Stirring Casting Process on the Mechanical Properties of $SiC_p$/A356 Composites.* Stirring temperature significantly affects the uniformity of SiC particles in stirring prepared $SiC_p$/A356 composites. The influence of stirring temperature on SiC particle distribution uniformity is shown in Figure 3. The melts did not undergo refining treatment during the processing of composites. As shown in Figures 3(a)–3(d), the aggregation of SiC particles intensified at a stirring temperature of 750°C. The aggregates were accompanied by pores, even inclusions, which makes them more similar to the "impurity pores" defects in casting. These "impurity pores" were probably not generated during solidification but during the stirring preparation of $SiC_p$/A356 composites, considering the high thermal conductivity of the casting molds. As shown in Figure 3(b), pores still appear in the composites at 700°C, and circular aggregation of SiC

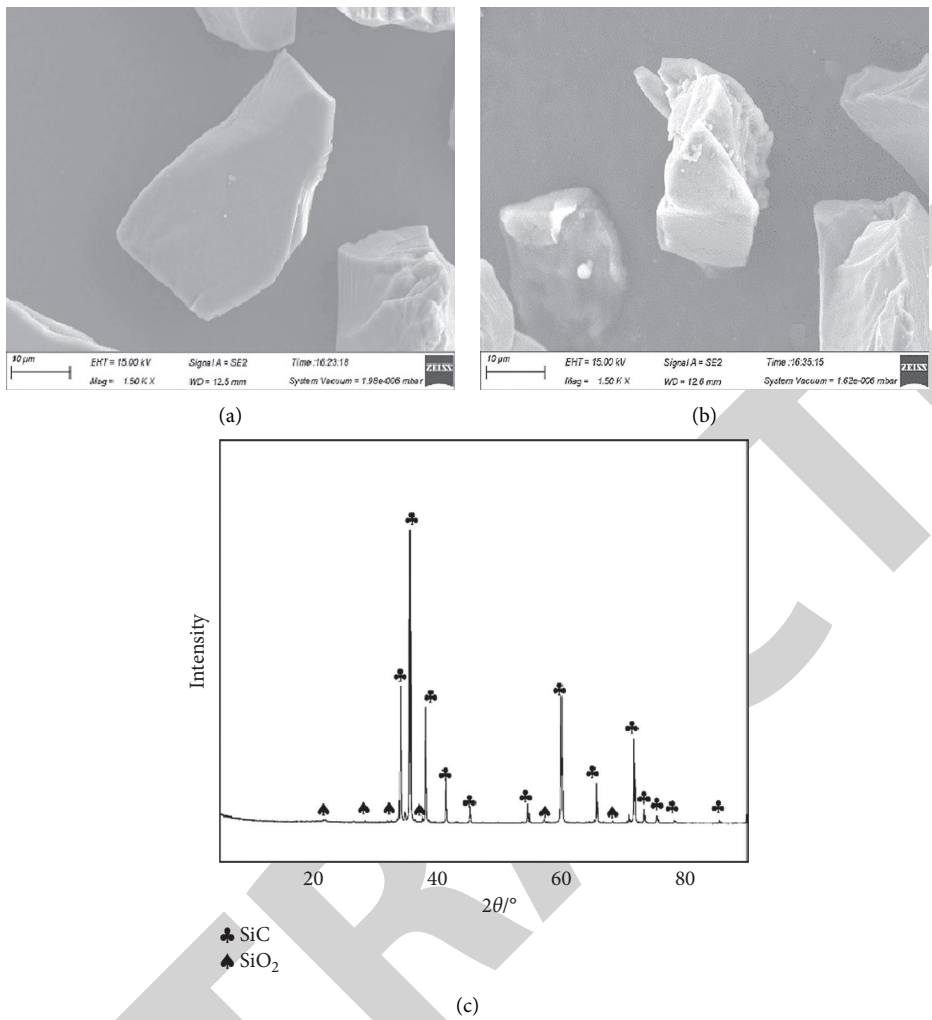


Figure 1: Microstructure of the SiC particles: (a) untreated and (b) oxidation-treated; (c) X-ray diffraction of SiC particles after oxidation treatment.

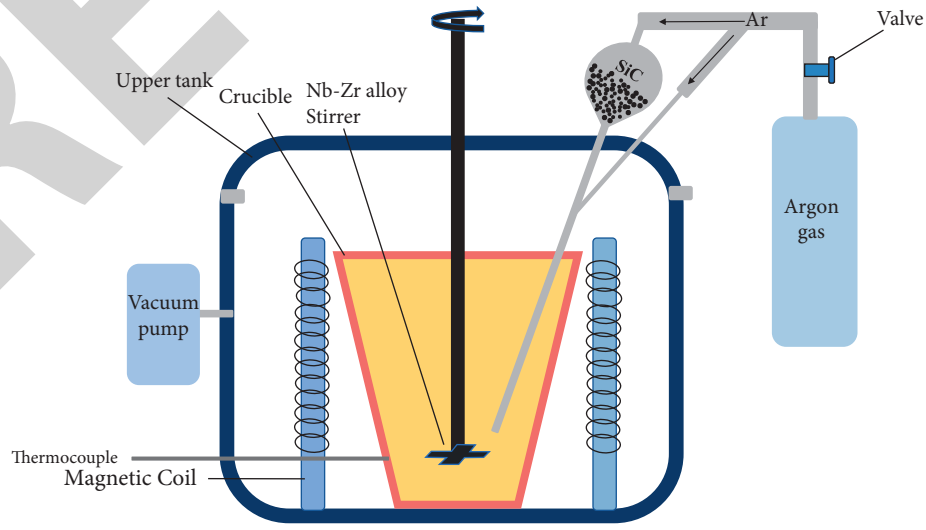


Figure 2: Schematic of the vacuum furnace.

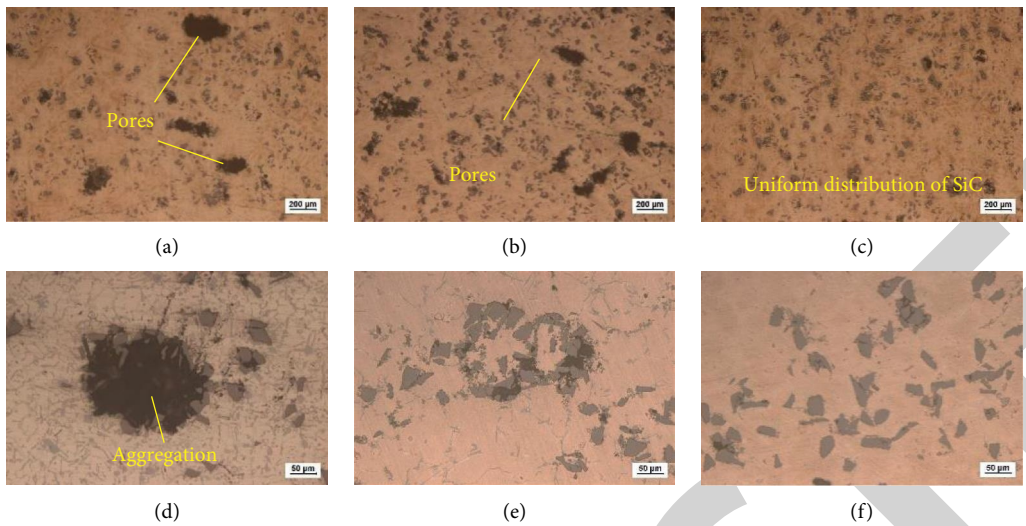


Figure 3: The effects of stirring temperature on the dispersion uniformity of SiC particles (a, d) 750°C; (b, e) 700°C; (c, f) 650°C.

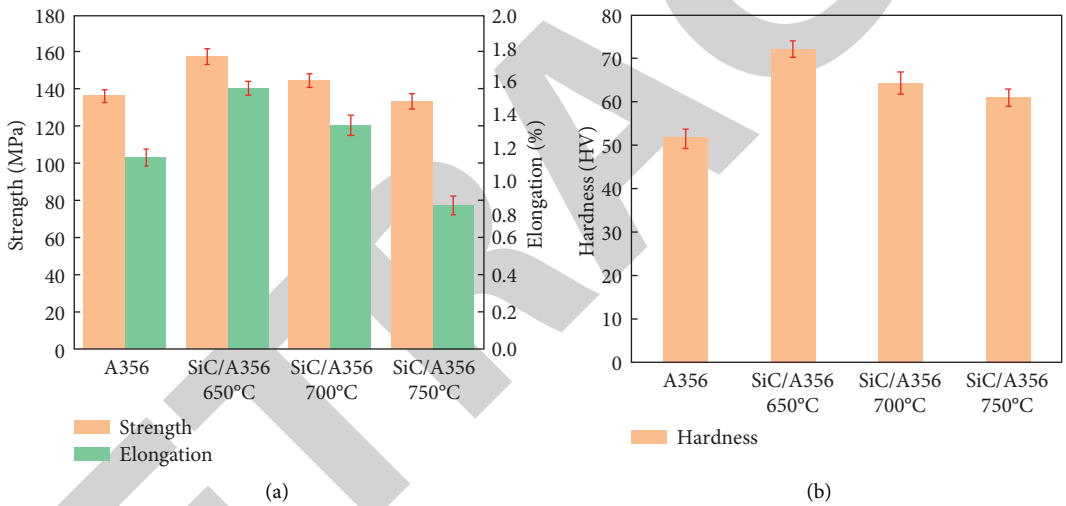


Figure 4: Mechanical properties of the $SiC_p$/A356 composites at different conditions: (a) tensile strength; (b) hardness.

particles seems to be the cause (Figure 3(e)). At a relatively lower stirring temperature, fewer "impurity pores" came into being and the uniformity of SiC particle distribution was increased. A uniform distribution of SiC particles was observed for the 650°C stirred sample in an increased quantity (Figure 3(c)). A large number of SiC particles exist in the matrix in isolation (Figure 3(d)). This may be due to the formation of a certain amount of primary $\alpha$-Al phase in the matrix when stirred at 650°C, but due to the low volume fraction, the grain size is relatively small, and it is difficult to observe in the solidified structure. These fine primary particles in the stirring of SiC particle clusters impact and friction and promote its dispersion; at this time, the melt viscosity is significantly increased than the complete liquid; in the same stirring speed, the higher the melt viscosity, the greater the internal friction formed.

Figure 4 illustrates the effects of stirring temperature on the mechanical properties of the $SiC_p$/A356 composites. As shown in Figure 4(a), tensile properties of the $SiC_p$/A356 composites did not exhibit noticeable improvement compared to A356 alloy, except for the sample prepared at a stirring temperature of 650°C. The elongation of the 750°C sample was even lower than that of the A356 alloy. Overall, the $SiC_p$/A356 composites have shown enhanced hardness over the A356 alloy (Figure 4(b)).

Figure 5 shows the fracture morphology at stirring temperatures of 750°C and 650°C. When the stirring temperature was 750°C, there were obvious defects such as pores on the fracture. These pores expanded into cracks during the loading stress process, which greatly reduced the plasticity of the composite compared with the matrix alloy and led to the decline of the elongation of the sample. At the stirring temperature was 650°C, the porosity of the composites was greatly reduced, and many dimples appeared. The composites show the characteristics of ductile fracture locally. As shown in Figure 4, the elongation of the sample is also much

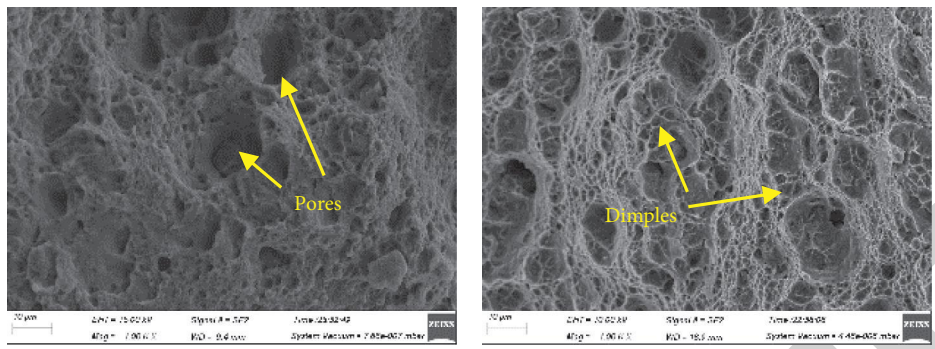


(a) (b)

Figure 5: Fracture morphology at different stirring temperatures: (a) 750°C; (b) 650°C.

higher than that of the composite material prepared at 750°C.

*3.2. The Effects of Oxidation of SiC at High Temperature.* It is difficult to guarantee the uniform dispersion of SiC particles in the matrix of $SiC_p$/Al composites by traditional processing techniques. Thereby, special processes such as vacuum stirring are necessary for the manipulation of SiC particle input. That said, aiding methods to increase the wettability of SiC particle/Al melt and suppress the interfacial reactions during preparation, including modification of SiC particles or alloy element addition, are still inevitable to facilitate the blending of particles into Al melt, resulting from the difficulty in the blending of SiC particles and Al melt. Here, oxidation of SiC at high temperature was adopted for SiC modification [14]. The morphology of the modified SiC particles was revealed by SEM images in Figure 6. The $SiO_2$ layer formed on the surface of SiC particles can increase the interfacial wettability, while the $SiO_2$ layer might undergo the following reactions during vacuum stirring and the $MgAl_2O_4$ phase was detected at the $SiC_p$/Al interface, indicating that the $SiO_2$ generated on the surface of SiC reacts with Al and Mg in the aluminum liquid after oxidation, and eventually $MgAl_2O_4$ is formed near SiC [15]:

$$SiO_2 + Al + Mg \longrightarrow MgAl_2O_4 + Si \quad (1)$$

The interface reactions in question might facilitate the uniform distribution of SiC particles under certain circumstances. It has been reported that reaction (1) occurs at high temperatures (750°C), which indicates that the possibility of a reaction (1) increased with vacuum stirring temperature during stirring preparation of the $SiC_p$/A356 composites. Slight oxidation of SiC particles promoted particle blending and the uniform particle distribution in the matrix after solidification. However, with a stirring temperature higher than 750°C, overoxidation of SiC particles would occur, leading to the adsorption or generation of $Al_2O_3$ or MgO around the particles. It is easy for oxidated SiC particles to be absorbed by oxide inclusions. Such oxide inclusions would further trap other oxide inclusions in the Al melt (Figure 3(d)) or even capture SiC particles and

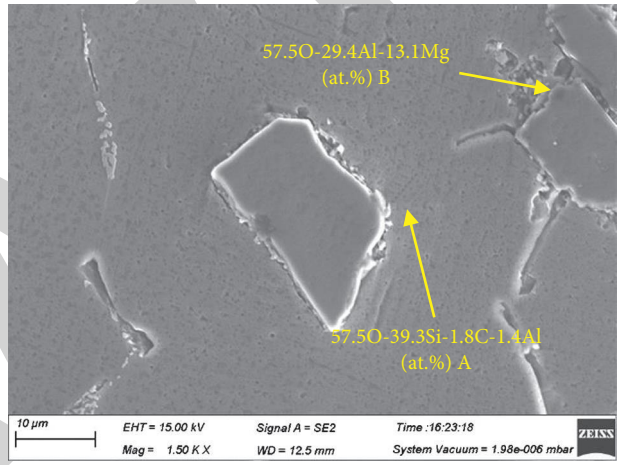


Figure 6: SEM images and EDS results of $SiO_2$ layer (a) and $MgAl_2O_4$ phase near SiC (b).

gradually grow to large oxide inclusion lumps. With a higher density than that of Al melt, the oxide inclusions would be thrown out of the liquid surface by centrifugal force and float on the Al melt surface for surface tension. Therefore, a large amount of SiC particles would be consumed, leading to lowered SiC particle content in the final $SiC_p$/Al composites. Longer stirring time leads to exaggerated consumption of SiC particles. During casting, gas flows in rapidly once the upper tank is open. If the oxide inclusion lumps containing SiC particles are scattered by the blades and suspended inside the Al melt, these oxide inclusions absorb gas easily as the gas content of the Al melt increases dramatically. After solidification, around $Al_2O_3$ inclusions where SiC is absorbed, pores or shrinkage defects would be generated (Figures 3(a)–3(b)).

*3.3. The Effects of the Rare Earth Element Sc on the Mechanical Properties of $SiC_p$/A356 Composites.* The results in Section 3.1 confirm that the $SiC_p$/A356 composite prepared at a stirring temperature of 650°C showed a high SiC particle content with a uniform distribution, while the inclusion content was relatively low. Therefore, further experiments were conducted with this composite material. Inoculation

and refining treatments are key processes for microstructure improvement and mechanical property enhancement in the melting of casting Al-Si alloy [16]. Obvious inoculation effects can be obtained from Na and Sr elements. However, the short inoculation time of Na tends to generate inclusions [17], while Sr offers a longer inoculation time but tends to cause gas absorption and oxidation film generation like $Al_2SrO_3$ and the increase in the pinhole tendency of the cast [18, 19]. By comparison, as a rare earth element, with a small amount of addition to Al alloy, the rare earth element Sc can pose refining and inoculating effects on the primary $\alpha$-Al and the eutectic Si phases of the alloy, accompanied by minimal inclusions. At 655°C, a eutectic reaction occurs after the addition of Sc : $L \longrightarrow \alpha + Al_3Sc$, where the Al3Sc particles serve as the heteronucleation sites for the primary $\alpha$ phase, significantly refining the cast microstructures [20]. SEM images depict the morphologies of $Al_3Sc$ and eutectic Si phases in the microstructures with the addition of Sc (Figure 7). As shown in Figure 7(a), $Al_3Sc$ existed in the cube shape, with a length of ~10 $\mu$m. As an intermetallic compound generated in situ in aluminum alloy, $Al_3Sc$ is characterized by a high melting point (1320°C), high stability, and uniform distribution. Once the Sc element was introduced to the composites, the eutectic Si grains were evidently refined and SiC particles showed up in the eutectic Si areas (Figure 7(b)). During solidification, with the growth of the primary phase $\alpha$-Al, the liquid phase with higher Si content pushes the SiC particles to the solidification front and gathers them together. When the temperature is further reduced, a eutectic reaction occurs, and because Si is diamond structured and very close to the sphalerite structured phase of SiC particles, and because SiC particles have rough surfaces and possess complex shapes, the last eutectic Si phase solidified in the melt will choose to preferentially nucleate on the surface of SiC particles. The existence of both $Al_3Sc$ and SiC was confirmed by XRD patterns of the samples (Figure 7(c))

Figure 8 shows the stress-strain curves of composites with different Sc content. It can be seen that the maximum tensile strength of $SiC_p$/A356 composites increases significantly with the increase of Sc content, but the elongation of SiCp/A356 composites gradually decreases with the increase of Sc content after the Sc content exceeds 0.4wt%. According to the Al-Sc binary phase diagram, it was known that after Sc reaches 0.55wt%, a certain percentage of Sc exists as precipitated secondary $Al_3Sc$ phase formation, and $Al_3Sc$ particles may form agglomerates at the grain boundaries, and these agglomerated tiny particles may act as a source of microcracks during the tensile process of the composites, which leads to the decrease of plasticity of the material.

The effects of addition temperature on the microstructure and SiC distribution of the $SiC_p$/A356 composites with 0.4 wt% Sc are illustrated in Figure 9. The addition of Sc resulted in the grain refinement of the primary $\alpha$-Al phase and the transformation of the eutectic Si shape from flakes to fibers (Figures 9(b) and 9(c)). SiC particles appeared in the eutectic Si areas, showing no obvious drop in the content in the samples. Compared with the samples shown in Figures 9(a) and 9(d), as the melt temperature elevated, the oxidation of the SiC particles intensified so that the SiC particles were covered by oxides (Figures 9(e) and 9(f)). It indicates that the SiC particles might undergo further oxidation in the form of reaction (1), leaving SiC in the final residual liquid region, the eutectic region, during solidification. When the composite was solidified, the SiC particles have a sphalerite structure, while the primary $\alpha$-Al has a face-centered cubic structure. The crystal structure of the SiC particles is quite different from that of the primary $\alpha$-Al, and the SiC particles cannot become the crystalline core of the primary $\alpha$-Al. Therefore, with the growth of the primary $\alpha$-Al phase during solidification, SiC particles are pushed and aggregated in the liquid phase with high Si content. When the temperature is further reduced, the eutectic reaction occurs because Si is of a diamond structure, which is close to the sphalerite structure of SiC particles, so SiC particles become the heteronucleation substrate of eutectic Si, and eutectic Si nucleates preferentially on the surface of SiC particles. As can be seen from Figures 9(d) and 9(e), after the addition of the rare earth element Sc, the coarse eutectic Si structure disappears and the eutectic Si structure is refined.

The effects of melt temperature and Sc addition on the mechanical properties of the $SiC_p$/A356 composites are examined in Figure 10. The $SiC_p$/A356 composites with 0.4 wt% Sc exhibited significantly enhanced tensile properties and hardness, among which the composites with 700°C addition temperature showed the maximum tensile properties of a 193.5 MPa tensile strength and a 3.2% ductility. The hardness tests revealed that the sample microhardness continually increased with the melt temperature, reaching 86 HV at 720°C.

Figure 11 shows the microstructure and EDS result $SiC_p$/A356 composites after adding Sc. SEM images show that an irregular massive phase exists at SiC particle/Al interface. The phase is attached to SiC particles, and EDS map analysis shows that the phase is a compound rich in rare earth element Sc. A compound was formed consisting of Al, Si, and Sc according to the EDS result. According to Figure 11(c), XRD analysis results show that the phase might be $Si_5Sc_3$. The tensile strength and hardness of the material have been increased due to this new phase. This may be because the phase increases the interfacial bonding strength.

Jadhav et al. [21] proposed three failure modes of particle reinforced composites under axial load, as shown in Figure 12: (a) fracture at particles; (b) fracture at matrix; (c) fracture at particle/matrix interface:

(a) When the local stress concentration exceeds the fracture strength of the SiC particles or when the SiC particles are defective, the particles fracture is reinforced. The microscopic cracks formed by the fractured particles expand through the association of microscopic pores in the collective and eventually cause the material to fracture and fail.

(b) When both the interfacial bond strength and the SiC particle fracture strength are very high, and there are no obvious defects in the material, the matrix first produces plastic failure, and the pores in the matrix nucleate,

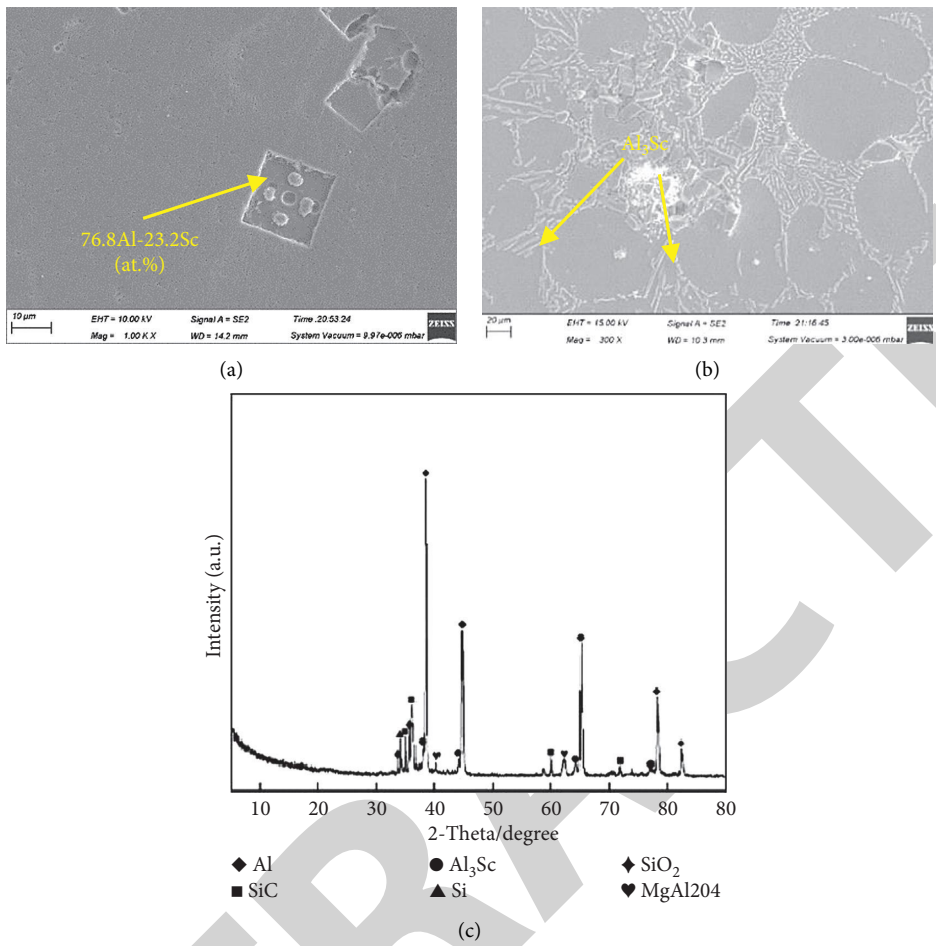


Figure 7: SEM images and EDS result (a) of $Al_3Sc$, microstructures after addition of Sc (b), and X-ray diffraction of 10%$SiC_p$/Al + 0.4Sc (c).

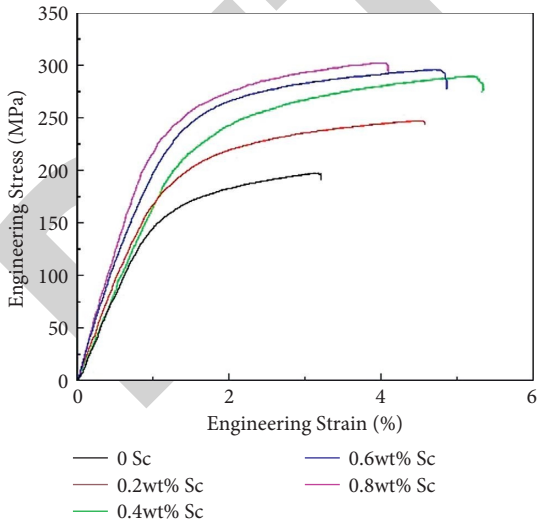


Figure 8: Stress-strain curves of composites with different Sc contents.

grow, and connect. After that, as the stress in the part of the material that is not fractured increases sharply, an interfacial separation between the particles and the matrix occurs, which finally leads to material failure.

(c) When the interfacial strength is lower than the SiC particle fracture strength and the local stress exceeds the interfacial strength, cracks are the first to develop at the SiC particle-matrix interface. The crack extension will connect through the pores at the interface and expand in the composite.

Figure 13(a) shows the fracture morphology of the composites without the addition of Sc. The fracture of SiCp/A356 composites after Sc modification is a mixture of ductile fracture with mainly brittle fracture and coexistence of brittle fracture. There is an obvious flat of SiC particles falling off on the fracture. The EDS analysis proved that the composition is at 99.6% Al. This phenomenon shows that when the sample was under load, the interface of SiC and Al was not strong, resulting in SiC particles falling off, which greatly reduces the plasticity of the composite compared with the matrix alloy, leading to the decrease of the elongation of the sample. Figure 13(b) shows the fracture of the composites when the Sc content is 0.4 wt%. It can be seen that the number and density of tough nests in the fracture are significantly increased, there are relatively clear tearing ribs around the tough nests, and the tough nests are relatively small and uniform, at which time the composites have a certain plasticity and better elongation than the composites of other compositions. Moreover, a fragment of SiC

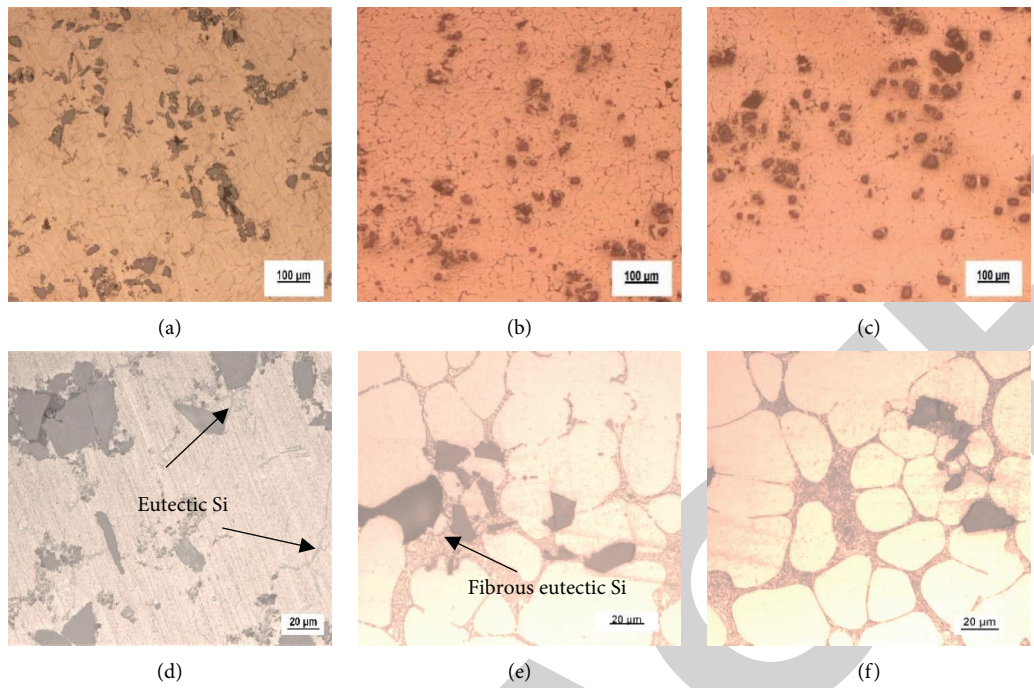


Figure 9: The effects of addition temperature on the microstructure and $SiC_p$ distribution: (a, d) without Sc addition; (b, e) 700°C; (c, f) 720°C.

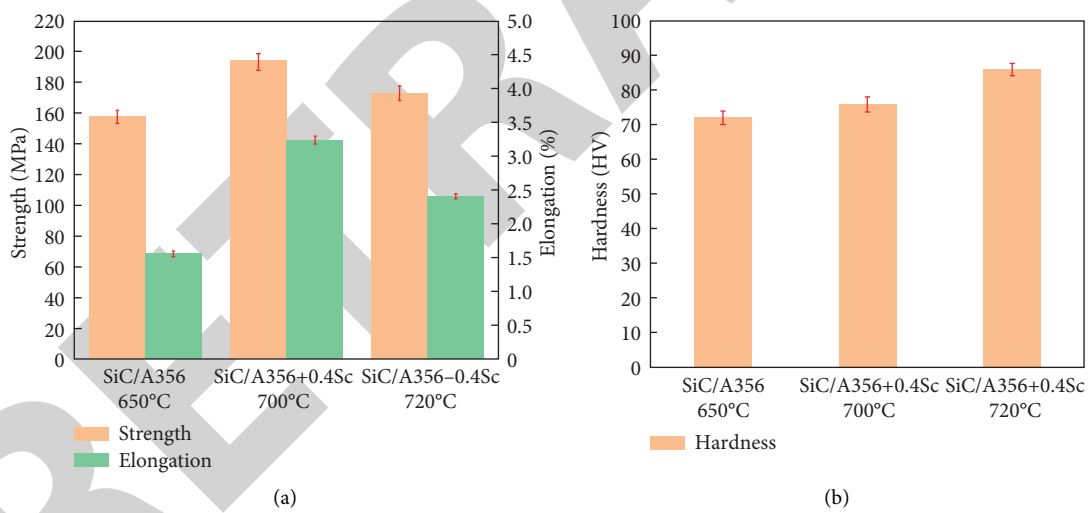


Figure 10: Mechanical properties of the $SiC_p$/A356 composites at different conditions: (a) tensile properties; (b) microhardness.

particle was found in Figure 13(b). It can be presumed that the strong bonding between the matrix/SiC interface and the stress could be effectively transferred to the reinforcement under load. Thus, the strength of the composites was improved.

## 4. Discussion

Based on the mechanical property tests, microstructure observation, and fracture analysis, the $SiC_p$/A356 composites showed trivial improvement in tensile strengthen after the addition of 10% $SiC_p$, which was related to the content, dispersion, and oxidation of SiC particles after vacuum stirring. The mechanical properties of SiCp/A356 composites depend to a large extent on the uniformity of SiC particle distribution and casting defects in the material. The more uniform the distribution of SiC particles in SiCp/A356 composites and the lack of defects such as oxidation inclusions and porosity, the better the mechanical properties of the composites. The high tensile strength of composites demands high content, small size, and uniform dispersion of SiC particles. On the one hand, the large particle size and low binding strength of matrix/SiC interfaces caused by inclusions and gas adsorption around the SiC particles explain the insignificant dispersion strengthening effect. On the other

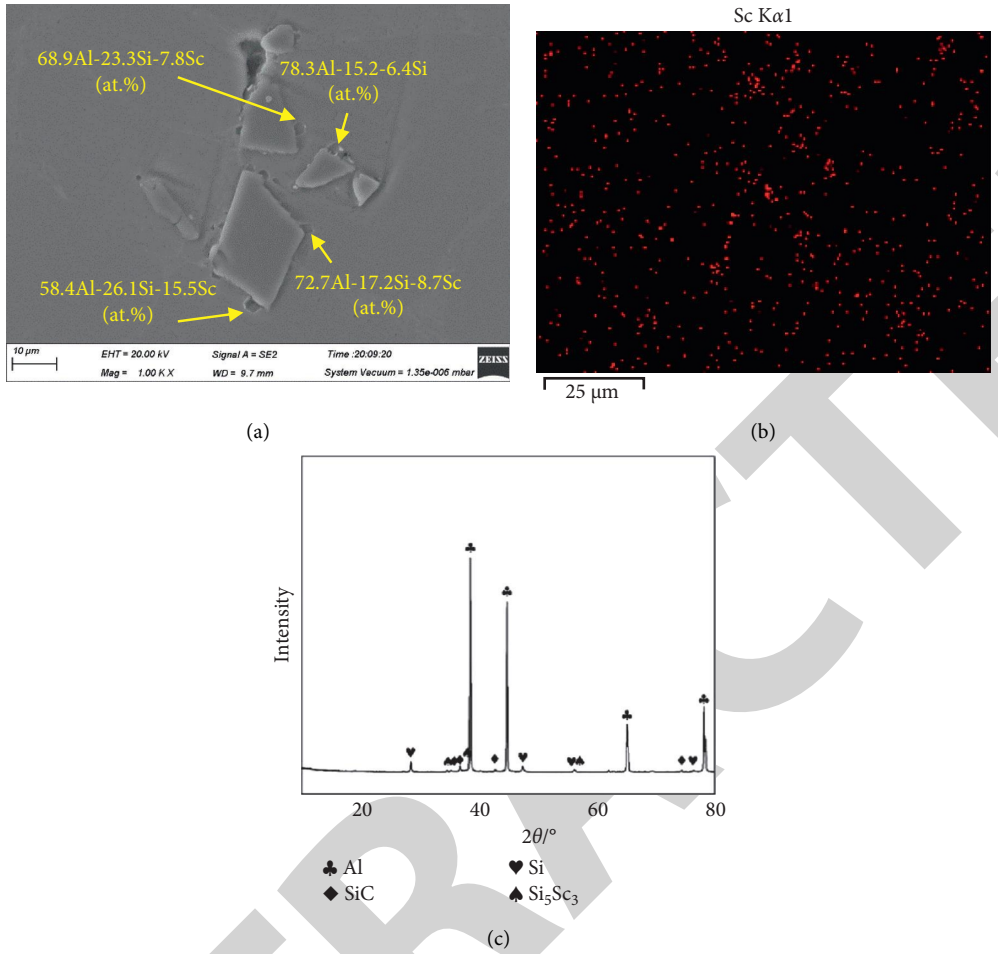


Figure 11: SEM image and EDS result of SiCp/A356 composites after adding Sc. (a) SEM image, (b) EDS map of Sc, and (c) XRD analysis.

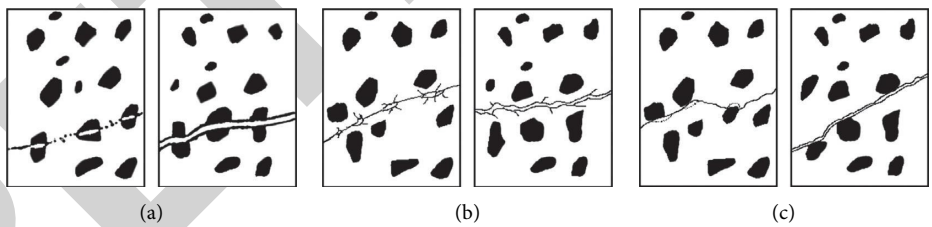


Figure 12: Different failure modes of particle reinforced composites.

hand, at the opening of the upper tank after stirring, the rapid gas influx to the Al melt led to gas adsorption of the SiC particles containing oxide inclusions, which multiplied the "impurity pores" in the obtained composites, resulting in the microcracks caused by stress concentration at the pore sites and thereby the premature fracture of the samples during tensile tests. Notably, the hardness of the composites surpasses that of A356 aluminum alloy, in contrast with the tensile properties. Especially, when the stirring temperature was 650°C, the HV of the sample reached ~70. Further increase in stirring temperature aggravated oxidation of SiC particles, the content of which dropped in the composites due to oxidation consumption, resulting in a significant decrease in hardness.

Research by Yang et al. [22] indicates that the non-uniform particle distribution caused by aggregation or segregation of SiC particles is one of the key factors for the decrease in the ductility and fracture toughness of $SiC_p$/Al composites. Our experiments demonstrate that one significant reason for the low ductility of the $SiC_p$/A356 composites is oxide inclusion induced SiC aggregation and the oxide inclusion adsorption around SiC particles. It compromises the binding strength of the $SiC_p$/Al interfaces, where microcracks tend to initiate and propagate, leading to the lowered ductility and explaining the premature fracture of samples. At a higher stirring temperature, SiC aggregation was exaggerated. The more the adsorbed oxide inclusions, the lower the ductility. The ductility was merely 0.9% when

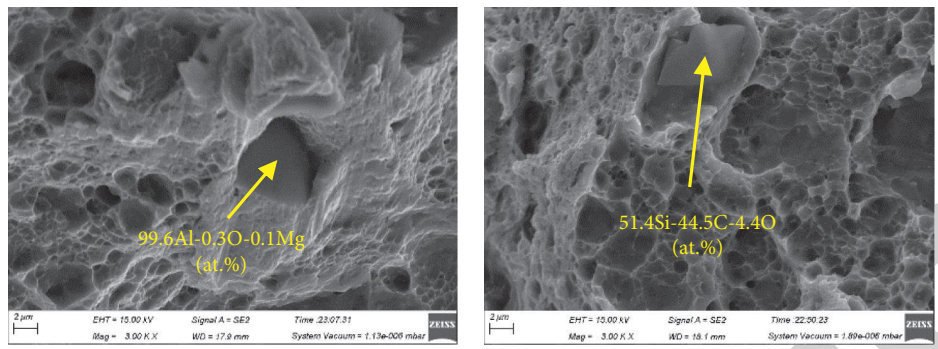


(a) (b)

Figure 13: The fracture morphology of the composites: (a) without Sc; (b) with Sc.

the samples were stirred at 750°C. The addition of Sc significantly improved the tensile strength and the ductility of the $SiC_p$/Al composites. After adding elemental Sc, the morphology of $\alpha$-Al grains changed, showing a clear elliptical profile, while the eutectic Si phase changed from coarse and long to fibrous. The reason for the strengthening effect lies in the grain refinement of primary $\alpha$-Al and the morphology change of eutectic Si with Sc addition. The dispersed eutectic $Al_3Sc$ phase inside the primary $\alpha$-Al phase enhanced the matrix of the composite. It can also be explained by the improved interfacial wettability of the SiC particles and the matrix caused by SiC oxidation, which enhanced the binding strength of $SiC_p$/Al interfaces. During tensile tests, microcracks were less likely to initiate on $SiC_p$/Al interfaces, accounting for the notable increase in tensile strength and ductility of the composites.

Obviously, the vacuum stirring prepared $SiC_p$/A356 composites without inoculation treatment exhibited scattered SiC distribution and SiC aggregation (Figure 3). The remelted composites treated with Sc saw a significant strengthening in the composite matrix. After Sc modification of the composite, a certain proportion of Sc exists in the form of precipitated secondary $Al_3Sc$ phase, and $Al_3Sc$ can refine the grain structure and improve the tensile strength of the composite, but these $Al_3Sc$ particles may form agglomerates at the grain boundaries, leading to a decrease in the plasticity of the material. At the same time, the further oxidation of SiC particles enhanced the interface wettability of SiC and the matrix, which contributed to the more diffused distribution of SiC particles. During solidification, SiC particles should be solidified simultaneously with the matrix and hence dispersed in the matrix, but why do the particles tend to distribute in the eutectic Si region. The main cause is quite likely to be the gas adsorption of oxidated SiC particles. The density of SiC particles dropped after adsorption so that the particles tended to be pushed to the residual liquid region by buoyancy force. The higher the melt temperature, the more intensified the oxidation of SiC particles and the more the adsorption of gas, leading to segregation even aggregation of SiC particles in the residual liquid region, which accounted for the failure in dispersion strengthening of SiC particles on the matrix. Therefore, the tensile strength and ductility of the composites decreased (Figure 10(a)). However, the high melt temperature is in favor of Sc diffusion and beneficial for the matrix strengthening.

## 5. Conclusions

In our work, 10 vol.% $SiC_p$/A356 composites were prepared under a vacuum condition. This vacuum stirring cast process and rare earth element treatment can provide technical reference for dealing with the problem of fabrication of $SiC_p$/Al MMCs. The main observations are summarized as follows:

(1) In vacuum stirring preparation of $SiC_p$/Al composites, high-temperature oxidation was utilized for SiC particle modification to increase the SiC particle/Al melt wettability. Overoxidation might occur during vacuum stirring, causing SiC loss and the increase in the amount of "impurity pores" or aggregation of SiC particles in the obtained $SiC_p$/Al composites. At the stirring temperature of 650°C, SiC particles were observed in a uniform distribution.

(2) After the Sc addition treatment on the remelted composites, significant strengthening was achieved on the composite matrix. The tensile strength was increased by 43% compared with the matrix alloy. After adding Sc, the $\alpha$-Al and eutectic Si were obviously refined.

(3) New phase $Si_5Sc_3$ was formed at the interface between Al and SiC particles, which may increase the interfacial bonding strength.

(4) A fracture at particles was detected after Sc addition treatment. The stress could be effectively transferred to the SiC particles when the fracture occurred.

## Data Availability

The labeled dataset used to support the findings of this study is available from the corresponding author upon request.

## Conflicts of Interest

The authors declare no conflicts of interest.

## Acknowledgments

This work was supported by the Key Science and Technology Project of Henan Province, under No. 182102210312, and Key Research Fund of Higher Education Institutions of Henan Province, under No. 15A430007.

## References

[1] T. J. A. Doel, M. H. Loretto, and P. Bowen, "Mechanical properties of aluminium-based particulate metal-matrix composites," *Composites*, vol. 24, no. 3, pp. 270–275, 1993.

[2] D. J. Lloyd, "Particle reinforced aluminium and magnesium matrix composites," *International Materials Reviews*, vol. 1, no. 39, pp. 1–23, 1994.

[3] M. Tan, Q. Xin, Z. Li, and B. Y. Zong, "Mechanical properties of aluminium-based particulate metal-matrix composites," *Journal of Materials Science*, vol. 36, no. 8, pp. 2045–2053, 2001.

[4] G. Fan, R. Xu, Z. Tan, D. Zhang, and Z. Li, "Development of flake powder metallurgy in fabricating metal matrix composites: a review," *Acta Metallurgica Sinica*, vol. 27, no. 5, pp. 806–815, 2014.

[5] W. Wu, B. Guo, Y. Xue, R. Shen, S. Ni, and M. Song, "Ni-AlxNiy core-shell structured particle reinforced Al-based composites fabricated by in-situ powder metallurgy technique," *Materials Chemistry and Physics*, vol. 160, pp. 352–358, 2015.

[6] Y. P. Sun, H. G. Yan, B. Su, L. Jin, and J. M. He, "Microstructure and mechanical properties of spray deposition Al/$SiC_p$ composite after hot extrusion," *Journal of Materials Engineering and Performance*, vol. 20, no. 9, pp. 1697–1702, 2011.

[7] H.-D. Wu, H. Zhang, S. Chen, and D.-F. Fu, "Flow stress behavior and processing map of extruded 7075Al/SiC particle reinforced composite prepared by spray deposition during hot compression," *Transactions of Nonferrous Metals Society of China*, vol. 25, no. 3, pp. 692–698, 2015.

[8] K. Wang, J. Cheng, W. Sun, and H. Xue, "An approach for increase of reinforcement content in particle rich zone of centrifugally cast $SiC_p$/Al composites," *Journal of Composite Materials*, vol. 46, no. 9, pp. 1021–1027, 2012.

[9] K. Wang, H.-S. Xue, M.-H. Zou, and C.-M. Liu, "Microstructural characteristics and properties in centrifugal casting of $SiC_p$/zl104 composite," *Transactions of Nonferrous Metals Society of China*, vol. 19, no. 6, pp. 1410–1415, 2009.

[10] M. Wu, X.-H. Qu, X.-B. He, Rafi-ud-din, S.-B. Ren, and M.-L. Qin, "Interfacial reactions between Sn-2.5ag-2.0ni solder and electroless Ni(P) deposited on $SiC_p$/Al composites," *Transactions of Nonferrous Metals Society of China*, vol. 20, no. 6, pp. 958–965, 2010.

[11] J. Hashim, L. Looney, and M. S. J. Hashmi, "The enhancement of wettability of sic particles in cast aluminium matrix composites," *Journal of Materials Processing Technology*, vol. 119, pp. 329–335, 2001.

[12] S. B. Prabu, L. Karunamoorthy, S. Kathiresan, and B. Mohan, "Influence of stirring speed and stirring time on distribution of particles in cast metal matrix composite," *Journal of Materials Processing Technology*, vol. 171, no. 2, pp. 268–273, 2006.

[13] K. Amouri, S. Kazemi, A. Momeni, and M. Kazazi, "Microstructure and mechanical properties of Al-Nano/Micro sic composites produced by stir casting technique," *Materials Science and Engineering A*, vol. 674, pp. 569–578, 2016.

[14] V. Laurent, D. Chatain, and N. Eustathopoulos, "Wettability of $SiO_2$ and oxidized sic by aluminium," *Materials Science and Engineering A*, vol. 135, pp. 89–94, 1991.

[15] K. Wang, W. Li, J. Du, L. Yang, and P. Tang, "Thermal analysis of in-situ $Al_2O_3/SiO_2$(p)/Al composites fabricated by stir casting process," *Thermochimica Acta*, vol. 641, pp. 29–38, 2016.

[16] R. Haghayeghi and G. Timelli, "An investigation on primary Si refinement by Sr and Sb additions in a hypereutectic Al-Si alloy," *Materials Letters*, vol. 283, p. 128779, 2021.

[17] D. Emadi, J. E. Gruzleski, and J. M. Toguri, "The effect of Na and Sr modification on surface tension and volumetric shrinkage of A356 alloy and their influence on porosity formation," *Metallurgical Transactions A B*, vol. 24, no. 6, pp. 1055–1063, 1993.

[18] Y. Deng, Z. Yin, K. Zhao, J. Duan, and Z. He, "Effects of Sc and Zr microalloying additions on the microstructure and mechanical properties of new Al-Zn-Mg alloys," *Journal of Alloys and Compounds*, vol. 530, pp. 71–80, 2012.

[19] M. Zuo, D. Zhao, X. Teng, H. Geng, and Z. Zhang, "Effect of P and Sr complex modification on Si phase in hypereutectic Al-30Si alloys," *Materials & Design*, vol. 47, pp. 857–864, 2013.

[20] Y. K. Ma, Y. N. Liu, and M. X. Wang, "Microstructures and corrosion resistances of hypoeutectic Al-6.5si-0.45 Mg casting alloy with addition of Sc and Zr," *Materials Chemistry and Physics*, vol. 276, 2022.

[21] P. R. Jadhav, B. R. Sridhar, M. Nagaral, and J. I. Harti, "Mechanical behavior and fractography of graphite and boron carbide particulates reinforced A356 alloy hybrid metal matrix composites," *Advanced Composites and Hybrid Materials*, vol. 3, no. 1, pp. 114–119, 2020.

[22] N. Yang, J. Boselli, P. J. Gregson, and I. Sinclair, "Simulation and quantitative assessment of finite-size particle distributions in metal matrix composites," *Materials Science and Technology*, vol. 16, no. 7-8, pp. 797–805, 2013.